Journal of Sound and Vibration (2002) **251**(1), 115–139
doi:10.1006/jsvi.2001.3980, available online at http://www.idealibrary.com on IDEAL®

A HYBRID MODEL FOR THE NOISE GENERATION DUE TO RAILWAY WHEEL FLATS

T. X. Wu and D. J. Thompson

Institute of Sound and Vibration Research, University of Southampton, Southampton SO17 1BJ, England. E-mail: djt@isvr.soton.ac.uk

(*Received* 28 *March* 2001, *and in final form* 14 *August* 2001)

A numerical model is developed to predict the wheel/rail dynamic interaction occurring due to excitation by wheel flats. A relative displacement excitation is introduced between the wheel and rail that differs from the geometric form of the wheel flat due to the finite curvature of the wheel. To allow for the non-linearity of the contact spring and the possibility of loss of contact between the wheel and the rail, a time-domain model is used to calculate the interaction force. This includes simplified dynamic models of the wheel and the track. In order to predict the consequent noise radiation, the wheel/rail interaction force is transformed into the frequency domain and then converted back to an equivalent roughness spectrum. This spectrum is used as the input to a linear, frequency-domain model of wheel/rail interaction to predict the noise. The noise level due to wheel flat excitation is found to increase with the train speed V at a rate of about $20 \log_{10} V$ whereas rolling noise due to roughness excitation generally increases at about $30 \log_{10} V$. For all speeds up to at least 200 km/h the noise from typical flats exceeds that due to normal levels of roughness. When the wheel load is doubled the predicted impact noise increases by about 3 dB.

1. INTRODUCTION

When the brakes are applied to a railway wheel, it can sometimes happen that the wheel locks and slides along the rail. The reason for this may be poorly adjusted, defective or frozen brakes or lack of adhesion at the wheel/rail interface, for example, due to leaves on the rail head. This sliding causes severe wear of the part of the wheel in contact with the rail, leading to the formation of a "wheel flat". Such flats on the wheel may be typically 50 mm long but can extend to over 100 mm long. When the wheels subsequently rotate, these discontinuities on the wheel surface generate large impact forces between the wheel and track. As a consequence, a periodic impact noise is produced in addition to the usual rolling noise, which is more random and stationary in character. The large-amplitude dynamic forces generated by wheel flats may cause damage to the track, for example, resulting in fatigue cracks in the rails or sleepers. The high temperatures reached during sliding, followed by a rapid cooling, lead to the formation of brittle martensite within the steel beneath the wheel flat. As a result, damage to the wheel can also occur, involving cracking and spalling, that is the loss of relatively large pieces of metal [1].

A detailed study of the dynamic interaction between a wheel and the track in response to wheel flats was carried out by Newton and Clark [2], including both predictions and measurements. Their model was composed of (1) the vehicle, consisting of three masses representing the car body, bogie and wheel, plus primary and secondary suspensions, (2) a non-linear Hertzian contact spring between the wheel and the rail, and (3) the track, consisting of an infinite rail on an elastic foundation. In the field test, instead of using

0022-460X/02/110115 + 25 $35.00/0

a wheel flat, an equivalent indentation was placed in the railhead. This overcomes the difficulties in locating the position of the flats and their impacts relative to the instrumentation on the track. The indentation was intended to correspond to a rolling wheel with a "rounded flat", that is one which has undergone further rolling after formation, leading to rounding of the corners and extension of the effective length. Predictions in terms of the ratio of the peak contact force to the static wheel load showed good agreement with the measurements for train speeds up to about 80 km/h. It was shown that the impact force due to the assumed wheel flat increased with increasing train speed and had a peak at about 30 km/h, then decreased slightly up to 60 km/h and increased again thereafter. This observation was consistent with the results of a field experiment reported by the AAR [3]. Although the Newton and Clark work is not related directly to the issue of noise generation, it provides a basis on which to begin a detailed model of impact noise due to wheel flats.

A comprehensive study was carried out by Vér *et al.* [4] on estimating impact noise generation due to wheel and rail discontinuities. They established the concept of a critical speed, defined as the speed above which loss of contact occurs between the wheel and the rail. They also developed simple formulae for the critical speed, the rail impulse and the speed dependence of the sound power level for five types of discontinuity on the wheel or rail. Remington [5] extended this work and estimated an equivalent roughness spectrum corresponding to wheel flats or rail joints. This allowed the significance of any wheel flat or rail joint to be assessed in terms of its average noise generation capability, in comparison with roughness spectra measured on wheels and rails without significant defects.

The aim of this paper is to explore impact noise generation due to wheel flats more precisely and in detail. In order to calculate the wheel/track interaction force, a simplified track model is developed and combined with the wheel through a non-linear Hertzian contact stiffness. From the combined system of the wheel, contact stiffness and track, dynamic interactions between the wheel and rail are simulated in the time domain. The results are then analyzed in the frequency domain and the results are compared for different types of wheel flat and different train speeds. The concept of an equivalent roughness spectrum, as in reference [5], is also used in this study. However, here this is not derived from the wheel flat geometry directly, but from the results of the time-domain calculation. Thus, it is used as a means of converting the wheel/rail interaction force into an equivalent roughness input. By using this equivalent roughness input in the Track–Wheel Interaction Noise Software (TWINS) [6, 7] calculation model, the noise radiation from both wheel and track is predicted for excitation by wheel flats having different shapes and sizes.

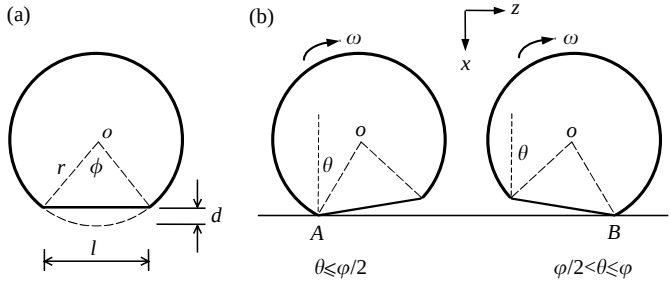

Figure 1. Rolling of a wheel with an idealized flat.

2. WHEEL FLAT EXCITATION

2.1. EXCITATION BY A NEW FLAT

Figure 1 shows a wheel with a newly formed flat rolling on a rail. The size of a wheel flat can be measured by its depth d and its length l. For an idealized flat, without any rounding or wear at its ends, these are related by $d \approx l^2/8r$ where r is the radius of the wheel. If a rigid wheel with such a flat rolls on a rigid rail without loss of contact, it will pivot about the "front" corner of the flat (A) until the flat is horizontal, and then pivot about the "rear" corner (B) until it can again roll on the round part of the wheel, see Figure 1(b). As a result the wheel centre falls initially, and then rises again.

From geometrical considerations, the vertical movement of the wheel centre, x_0 (positive downwards) is given by

$$x_0 = \begin{cases} r(1-\cos\theta) & 0 \leqslant \theta \leqslant \varphi/2 \\ r[1-\cos(\varphi-\theta)], & \varphi/2 < \theta \leqslant \varphi \end{cases}, \tag{1}$$

where $\varphi = 2\cos^{-1}[(r-d)/r]$ is the angle subtended by the flat at the wheel centre and is dependent on the wheel radius and flat size. x_0 will be termed the wheel centre "trajectory".

As the flat depth d is much smaller than the wheel radius r, the angle φ is small and equation (1) can be approximately expressed in terms of the longitudinal position of the wheel centre, $z_0 = r\theta$,

$$x_0 = \begin{cases} z_0^2/2r & 0 \leqslant z_0 \leqslant l/2 \\ (l-z_0)^2/2r, & l/2 < z_0 \leqslant l \end{cases}. \tag{2}$$

This vertical motion of the wheel centre corresponds to a transient vibration, excited by the wheel flat. Clearly, the motion x_0 differs from the shape of the wheel flat itself, due to the finite size of the wheel. A similar effect is noted when a random roughness function excites the wheel/rail system: a modification of this roughness due to the curvature of the wheel has to be allowed for in determining the actual excitation for rolling noise calculations [8].

Figure 2(a) shows the shape of the wheel with a new flat as well as that of a round wheel, with the vertical scale exaggerated. The shape of the flat can be expressed as a profile height, x_p, which is the difference between the two curves in Figure 2(a). This is given by

$$x_p(z) \approx \frac{1}{2r}\left(\frac{l^2}{4} - \left(z - \frac{l}{2}\right)^2\right) = d - \frac{1}{2r}\left(z - \frac{l}{2}\right)^2, \quad 0 \leqslant z \leqslant l, \tag{3}$$

where z is the circumferential distance along the wheel surface. This is the profile that would be measured by a probe with a small radius of curvature. The profile, x_p, and the wheel centre trajectory, x_0, are compared in Figure 2(b) from which it can be seen that the lengths and depths are both equal, but that the trajectory, x_0, has a quite different shape to the flat geometry, x_p.

As neither the track nor the wheel are rigid, the actual motion of the wheel centre is much more complicated than that described in equation (2). However, equation (2) also represents the *relative displacement* excitation that occurs between a flexible track and wheel, in the same way as the roughness forms the input for rolling noise calculations [7]. If the train speed is high, loss of contact may occur, and an impact between the wheel and rail occurs when the wheel hits the rail again; nevertheless, loss of contact is allowed for within the contact spring (see section 3) and does not affect the form of the input defined by equation (2).

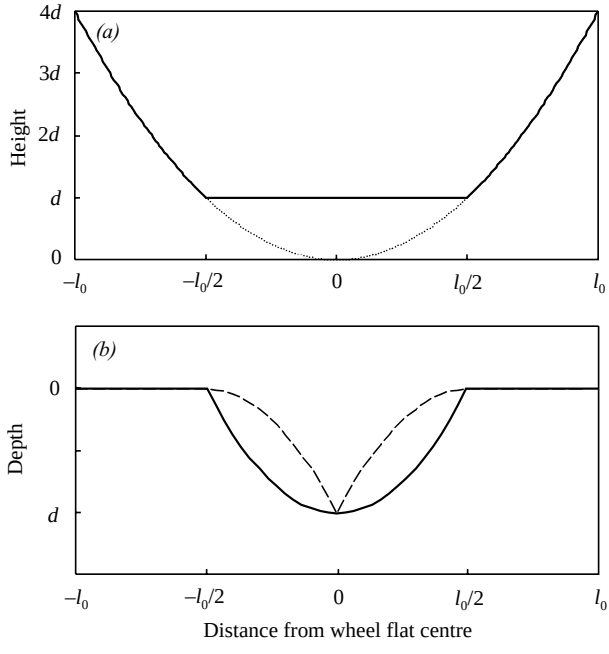

Figure 2. Wheel flat geometry for new flat of length l_0, (a) Wheel geometry: ——, with flat; · · · · ·, round wheel; (b) with wheel curvature removed: ——, profile depth, – – –, wheel centre trajectory.

2.2. EXCITATION BY A ROUNDED FLAT

In practice, due to continued running of the wheel after formation of the flat, the profile becomes rounded at the corners of the flat, whereas the central part will remain unchanged. The overall length of the rounded flat, l, will be greater than that for a new flat of the same depth, l_0. Figure 3(a) shows three such rounded flats with the same depth, d, but different lengths, l.

If it can be assumed that these rounded corners can be represented by a *quadratic* function with smooth transitions, it is shown in Appendix A that the wheel centre trajectory will be described by

$$x_0 \approx \begin{cases} 4d\,(z_0/l)^2, & 0 \leqslant z_0 \leqslant l/2 \\ 4d((l - z_0)/l)^2, & l/2 < z_0 \leqslant l \end{cases}. \tag{4}$$

where l is the length of the rounded flat and d is the depth (which is no longer simply related to the length l). This expression clearly satisfies the requirements that $x_0 = 0$ at $z_0 = 0$ and at $z_0 = l$, and $x_0 = d$ and $z_0 = l/2$. In fact, equation (2) is a special case of equation (4) for the case $d = l^2/8r$. Thus, equation (4) can be used for both new flats and rounded flats of the type considered here.

Figure 3 shows the flat profile and the wheel centre trajectory for three idealized rounded flats. It can be seen that the wheel centre trajectories are identical to that in Figure 2 except that they are stretched in the z direction.

In practice, a rounded flat will differ in geometry from the idealized case considered here. However, in the absence of measured data, equation (4) will be used in this study to represent the dynamic excitation to the wheel/rail system. For measured flat profiles a numerical procedure can be employed to determine the wheel centre trajectory, similar to that used in reference [9] for roughness.

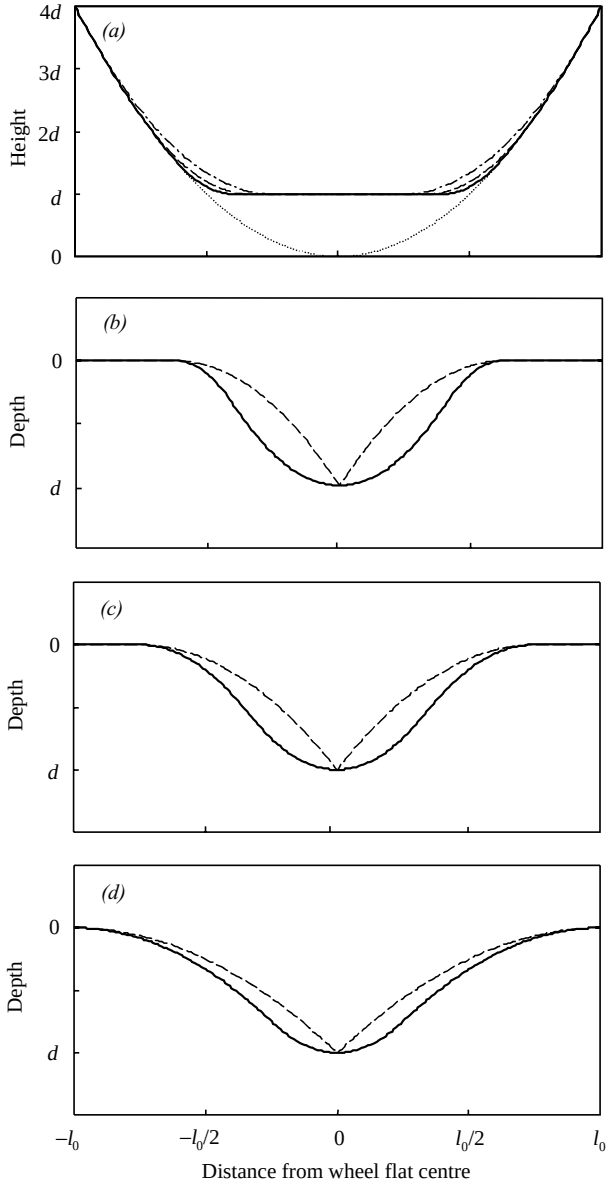

Figure 3. Wheel flat geometry for rounded flats. (a) Wheel shape for various rounded flats: ——, total length $l = 5l_0/4$; – – –, total length $l = 3l_0/2$, –·–·, total length $l = 2l_0$, with l_0 the length of the equivalent new flat. (b) Rounded flat, total length $l = 5l_0/4$: ——, profile depth (with wheel curvature removed): – – –, wheel centre trajectory. (c) Rounded flat, total length $l = 3l_0/2$, key as (b), (d) rounded flat, total length $l = 2l_0$, key as (b).

2.3. EXCITATION BY EQUIVALENT ROUNDED FLAT ON THE RAIL

It is also possible to consider a perfectly round wheel with an indentation on the railhead. This was used in the field tests in reference [2], where the following irregularity profile was introduced onto the railhead for the tests:

$$x_p(z) = \frac{d}{2}\left(1 - \cos 2\pi \frac{z}{l}\right), \tag{5}$$

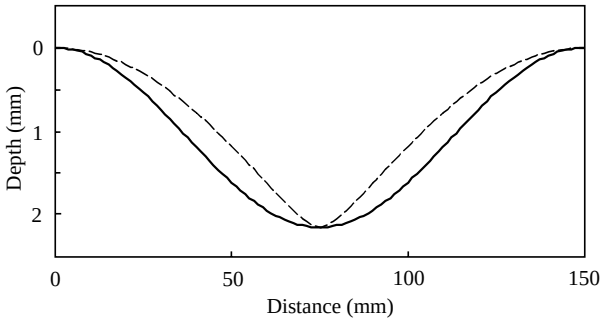

Figure 4. Wheel flat geometry from equation (5), $r = 460$ mm, $d = 2{\cdot}15$ mm and $l = 150$ mm: ——, irregularity on the railhead; – – –, wheel centre trajectory.

where the depth d was 2·15 mm and the overall length l was 150 mm. When a round wheel rolls over the curve described above, its centre trajectory can be given as

$$x_0(z_0) = x_p(z) + r(1 - \cos\theta), \tag{6a}$$

where z_0 is the longitudinal position of the wheel centre and z is the longitudinal position of the contact point on the rail, which are related by

$$z_0 = z + r\sin\theta \tag{6b}$$

and where

$$\theta \approx \tan\theta = x_p'(z) = \frac{\pi d}{l}\sin 2\pi\frac{z}{l}. \tag{6c}$$

These expressions are derived using the same method as given in Appendix A for the rounded flat of the last section.

Figure 4 shows both the irregularity curve described by equation (5) and the wheel centre trajectory calculated by using equations (6) for a wheel of radius 0·46 m. From this it is seen that the size of the wheel modifies the effective input provided by the irregularity (flat) in a similar way to that found above. However, the dimensions of the irregularity in reference [2] are such that the wheel can roll over the whole of the rail, i.e., if converted to an equivalent "flat" it would not be flat at its centre but slightly convex. As a result, the contact point does not jump along the rail, as before, and the trajectory is slightly rounded at its trough, unlike those in Figure 3.

3. WHEEL/RAIL INTERACTION MODEL

3.1. WHEEL/TRACK INTERACTION MODEL

The wheel/track interaction model is shown schematically in Figure 5. The vehicle system above the primary suspension is simplified to a static load W. This is justified as the vibration frequency of interest here is within the audio-frequency range, for example 50–5000 Hz, whilst the natural frequency of the vehicle suspension system is only a few Hertz, and thus the low-frequency vibration of the vehicle body and bogie is effectively isolated from the high-frequency vibration of the wheel and track. The track model is composed of an infinite Timoshenko beam on a continuous spring–mass–spring foundation representing the rail pads, sleepers and ballast respectively. Damping is introduced by adding loss factors to the pad and ballast stiffness. The wheel and rail are connected via

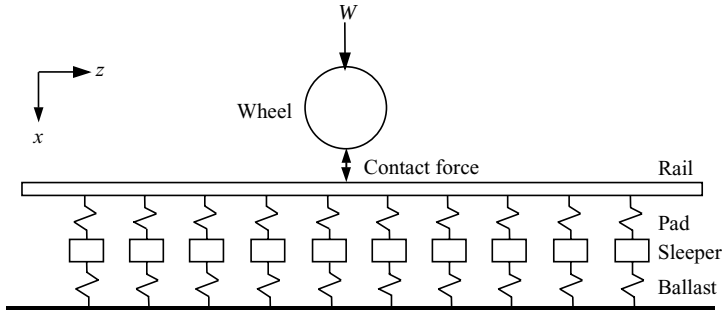

Figure 5. Wheel/track interaction model.

a Hertzian contact stiffness which is non-linear; the contact force is proportional to the elastic contact deflection to the power 3/2, provided that loss of contact does not occur.

As the train speed is much lower than the speed of flexural wave propagation in the rail in the frequency region of interest, a moving irregularity model can be used to simulate the wheel/rail interaction [10]. In such a model, the wheel remains stationary on the rail and an irregularity is effectively moved at the train speed between the wheel and rail as a relative displacement excitation. The source of vibration here is a wheel flat and the moving irregularity is represented by the "wheel centre trajectory", as calculated above.

Since the contact stiffness is non-linear and loss of contact may occur, it is necessary to calculate the wheel/rail dynamic interaction in the time domain. To do so, the main difficulties arise from the track model, because it is required that calculations are performed over an infinite spatial extent. On the other hand, the track model is considered to be linear and its dynamic properties are needed only at the contact position for the calculation of wheel/rail interactions. Thus, it is possible to develop an equivalent but much simpler system with only a single input (force) and a single output (displacement) to replace the track model represented in Figure 5. If this linear system has the same frequency response function (both amplitude and phase) as the track, it can be mathematically substituted for the track [11].

3.2. SIMPLIFIED TRACK MODEL

The vibration behaviour of the continuously supported Timoshenko beam model on the spring–mass–spring layers is similar to a two-degree-of-freedom system at low frequencies, because here the motion of the beam is strongly dependent on the foundation stiffness. At high frequencies, however, the beam vibration is coupled much more weakly to the foundation and it shows a free-beam like behaviour. In terms of the point receptance, such a track model can be approximated by a system with the following transfer (frequency response) function:

$$H(s) = \frac{X(s)}{F(s)} = \frac{b_1 s^3 + b_2 s^2 + b_3 s + b_4}{s^4 + a_1 s^3 + a_2 s^2 + a_3 s + a_4}, \tag{7}$$

where $X(s)$ and $F(s)$ are the Laplace transforms of the displacement (output) and force (input) at the contact position respectively. Constant coefficients a_i and b_i are determined by minimizing the differences between $H(\mathrm{i}\omega)$ and the point receptance of the track in the frequency region of interest.

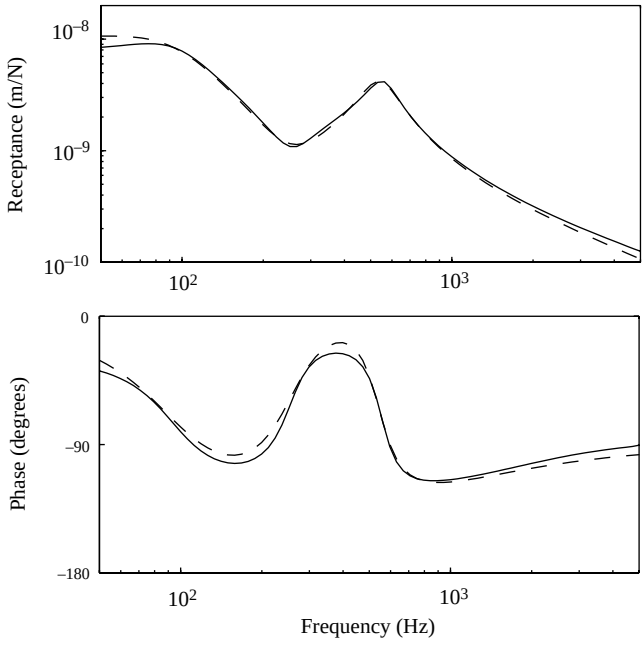

Figure 6. Amplitude and phase of the track frequency response function: ——, point receptance of the continuously supported track model; – – – –, frequency response function of the simplified track model, which is calculated by using equation (7), where $b_1 = 3{\cdot}28 \times 10^{-6}$, $b_2 = 1{\cdot}87 \times 10^{-2}$, $b_3 = 23{\cdot}6$, $b_4 = 3{\cdot}97 \times 10^4$, $a_1 = 1{\cdot}77 \times 10^3$, $a_2 = 1{\cdot}26 \times 10^7$, $a_3 = 7{\cdot}87 \times 10^9$, $a_4 = 3{\cdot}93 \times 10^{12}$.

TABLE 1

Parameters describing the track vertical dynamics

Young's modulus of rail (N/m^2)	E	$2{\cdot}1 \times 10^{11}$
Shear modulus of rail (N/m^2)	G	$0{\cdot}77 \times 10^{11}$
Density of rail (kg/m^3)	ρ	7850
Loss factor of rail	η_r	0·02
Cross-section area of rail (m^2)	A	$7{\cdot}69 \times 10^{-3}$
Second moment of area (m^4)	I	$30{\cdot}55 \times 10^{-6}$
Shear coefficient	κ	0·4
Pad stiffness per unit length of rail (N/m^2)	k_p	583×10^6
Pad loss factor	η_p	0·25
Sleeper mass (half, per unit length of rail) (kg/m)	m_s	270
Ballast stiffness per unit length of rail (N/m^2)	k_b	$83{\cdot}3 \times 10^6$
Ballast loss factor	η_b	1·0

Figure 6 (solid line) shows the point receptance of a track with the parameters described in Table 1. This represents a track with UIC 60 rail (60 kg/m) on monobloc concrete sleepers. For a sleeper spacing of 0·6 m the rail pad stiffness corresponds to 350 MN/m, which is typical of a moderately soft pad. Also shown in Figure 6 is the frequency response function of equation (7) (dashed line). It can be seen that $H(\mathrm{i}\omega)$ is in good agreement with the point receptance of the infinite track model in the frequency region 50–5000 Hz. Thus, the simple model described by equation (7) can be used to replace the infinite beam model in terms of its point receptance to calculate the dynamic interaction between the wheel and track.

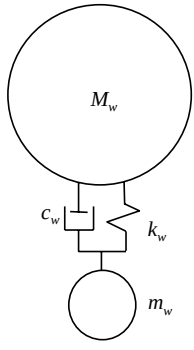

Figure 7. Simple wheel model. $M_w = 600$ kg, $m_w = 3$ kg, $k_w = 5$ GN/m, $c_w = 2\zeta\sqrt{k_w M_w}$ and $\zeta = 0{\cdot}025$.

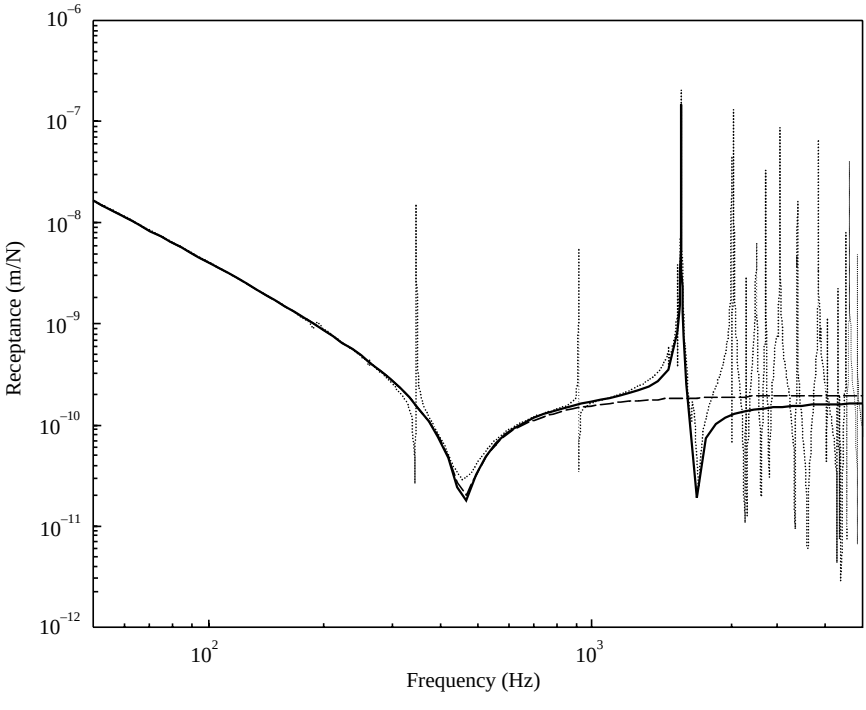

Figure 8. Wheel receptance for UIC 920 mm freight wheel: - - - -, simple model of Figure 7: ·····, full model from finite element mesh; ——, simplified modal model (section 5.3).

3.3. SIMPLIFIED WHEEL MODEL

The simplified wheel model is composed of two masses, a spring and a viscous damper, see Figure 7. The larger mass M_w is the unsprung mass of the wheel. The spring k_w is used to match the main trough around 460 Hz found in the measurements of the wheel receptance at the contact point. The damping c_w is used to reduce the sharpness of this trough. The small mass m_w is added, so that the wheel can be coupled with the track via a non-linear contact stiffness without mathematical difficulties. As this mass is very small, its influence on the wheel dynamic properties is negligible for frequencies below 10 kHz.

The deficiency of this simple wheel model is that the high-frequency modes of the wheel above 1 kHz are neglected. Figure 8 shows the wheel receptances of the simple model (dashed line) and of a full model based on a finite element prediction (dotted line). The third curve will be discussed later. It is seen that there are many resonant peaks and troughs in the full model which are not present in the simple model. The effects on the wheel/rail interaction of the high-frequency wheel modes, which are ignored due to the use of the simple model, may be considered using a special treatment, the use of an equivalent roughness excitation. This will be discussed in section 5.

4. SIMULATION OF WHEEL/RAIL INTERACTION DUE TO WHEEL FLATS

4.1. EQUATION OF MOTION FOR WHEEL/RAIL INTERACTION

The equivalent track model given by equations (7) can be expressed in the time domain by using a state-space form. Coupling the simplified track model with the wheel model through a Hertzian contact force, the equations of motion for the wheel/rail interaction can be written in the state-space form. The equations for the wheel are

$$\dot{x}_1 = x_2, \qquad \dot{x}_2 = [W - k_w(x_1 - x_3) - c_w(x_2 - x_4)]/M_w,$$
$$\dot{x}_3 = x_4, \qquad \dot{x}_4 = [k_w(x_1 - x_3) + c_w(x_2 - x_4) - f]/m_w, \tag{8a}$$

where x_3 is the wheel displacement (the displacement of the small mass m_w), x_1 is the displacement of the upper mass, W is the static load from the vehicle weight, and f is the non-linear wheel/rail interaction force. The rail motion is given by the state-space form of equations (7),

$$\begin{bmatrix} \dot{x}_5 \\ \dot{x}_6 \\ \dot{x}_7 \\ \dot{x}_8 \end{bmatrix} = \begin{bmatrix} -a_1 & 1 & 0 & 0 \\ -a_2 & 0 & 1 & 0 \\ -a_3 & 0 & 0 & 1 \\ -a_4 & 0 & 0 & 0 \end{bmatrix} \begin{bmatrix} x_5 \\ x_6 \\ x_7 \\ x_8 \end{bmatrix} + \begin{bmatrix} b_1 \\ b_2 \\ b_3 \\ b_4 \end{bmatrix} f, \tag{8b}$$

where x_5 is the rail displacement, and the interaction force is given by

$$f = \begin{cases} C_H(x_3 - x_5 - x_0)^{3/2}, & x_3 - x_5 - x_0 > 0 \\ 0, & x_3 - x_5 - x_0 \leqslant 0 \end{cases}, \tag{8c}$$

where x_0 is the relative displacement excitation due to the wheel flats, described for example in equation (4) for the idealized newly formed or rounded flats. Here x_0 is a function of time, and so becomes dependent on the train speed.

Simulations of the wheel/rail dynamic interaction have been carried out in the time domain by using the fourth order Runge–Kutta method with a constant time step.

4.2. COMPARISON WITH MEASURED IMPACT FORCE

Firstly, predictions from equations (8) are compared with the test results from reference [2] in terms of the ratio of the peak force to the static load, as validation of the above model. This is shown in Figure 9. The calculation parameters, including those for the track, are chosen here according to reference [2] and the relative displacement excitation, x_0, is calculated by using equations (5) and (6).

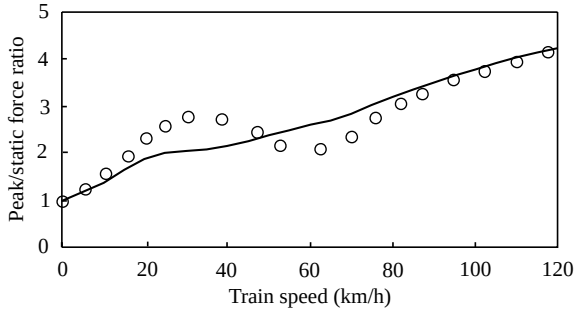

Figure 9. Comparison of the predictions with the field test results. Parameters used for predictions are from reference [2], with a railhead indentation input, $d = 2{\cdot}15$ mm, $l = 150$ mm. ——, predictions, ○ ○ ○, test results [2].

It can be seen that the predictions are very close to the test results for train speeds 0–15 and 80–120 km/h, whereas between 20 and 40 km/h the contact forces are underestimated by up to about 30%. It should be noted that, although the actual irregularity that was ground into the rail followed closely the form given in equation (5), some detail differences were present. Altogether, the level of agreement seen in Figure 9 is encouraging. In fact, the predictions using the simplified model are better than those in reference [2] which were based on three types of theoretical model for the track (an Euler beam on an elastic foundation, a Timoshenko beam on an elastic foundation and a discretely supported Euler beam).

4.3. IMPACT FORCE FOR WHEEL FLATS

Since the model represented in equations (8) is much simpler than the beam model it replaces, detailed simulations can be performed readily for different wheel flats and train speeds. Example results are presented in Figures 10 and 11 in terms of the wheel/rail interaction force, and the wheel and rail displacements at the contact position. Here, the static load from the vehicle weight is chosen as $W = 100$ kN, the wheel radius $r = 0{\cdot}46$ m, the wheel mass $M_w = 600$ kg and the Hertzian constant $C_H = 93{\cdot}7$ GN/m$^{3/2}$. The parameters for the track are given in Table 1.

Figure 10 shows the wheel/rail interaction due to a rounded wheel flat with depth $d = 2$ mm and length $l = 121$ mm. At a train speed of 30 km/h (Figure 10(a)), partial unloading occurs and the maximum contact force is about 3·5 times as large as the static load. When the indentation (relative displacement input due to the wheel flat) appears between the wheel and rail (the sign convention adopted is positive for an indentation and for downwards displacements), the wheel falls and the rail rises. Since the wheel and rail cannot immediately follow the indentation due to their inertia, the contact force is therefore partly unloaded. If the train speed is low, the static load is sufficient to maintain contact between the wheel and rail. After the relative displacement input reaches its maximum, the contact force increases rapidly until it reaches its peak. At this stage the relative displacement input decreases and the rail is forced to move downwards, but the wheel still keeps falling for a while due to its large inertia.

At a speed of 80 km/h (Figure 10(b)) loss of contact occurs twice. The first impact occurs at about 3·5 ms when the wheel hits the rail again after the first loss of contact. Here the force rises dramatically and the ratio of the peak force to static load is greater than 4. Since

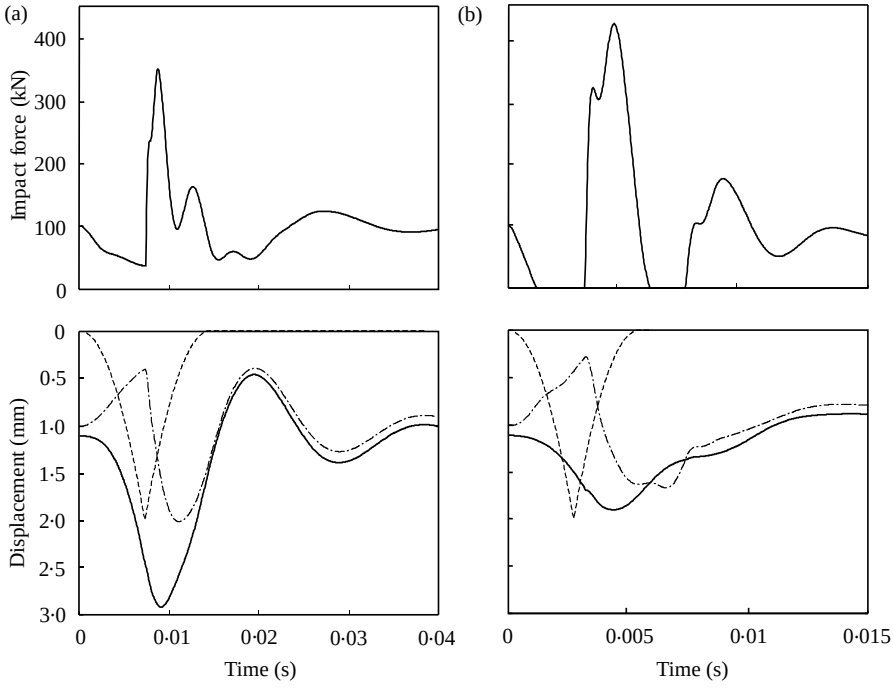

Figure 10. Wheel/rail interaction force (upper) and displacements of wheel and rail (lower) due to 2 mm rounded wheel flat. (a) At train speed 30 km/h. (b) At 80 km/h: ——, wheel displacement; – · – · –, rail displacement; ·····, relative displacement excitation.

the momentum of the wheel and rail are changed dramatically by the large impulse during this first impact, the wheel and rail are forced to move apart from each other and a second loss of contact occurs at about 6 ms. However, the second impact at 7·5 ms is much smaller than the first.

Figure 11 shows the results due to a newly formed wheel flat with depth $d = 2$ mm and length $l = 86$ mm. At a speed of 30 km/h (Figure 11(a)) slight loss of contact between the wheel and rail occurs. The maximum impact force here is larger than that for the rounded flat at 30 km/h, see Figure 10(a). This is because the duration of the displacement excitation here is shorter than for the rounded flat, while the peak values are the same for both, thus the accelerations of the wheel and rail are higher, and therefore the impact force is larger. At a speed of 80 km/h (Figure 11(b)), however, the impact force peak is smaller than that for the rounded flat. This is also because of the shorter duration of the relative displacement input. When the wheel contacts the rail again after loss of contact, the remaining displacement excitation is shorter and smaller compared with the rounded flat case, see Figures 10(b) and 11(b). As a result the impact force here is smaller.

The wheel/rail interaction force is periodic, repeating once every wheel revolution. In order to convert it to the frequency domain, a discrete Fourier transform is obtained of the force calculated for a whole wheel revolution. For example at a speed of 30 km/h, the fundamental frequency of this discrete spectrum is 2·88 Hz; at 120 km/h it is 11·5 Hz. These results are then converted to one-third octave band spectra in order to facilitate comparison between the results at different speeds. Figure 12 shows the force spectra produced from new and rounded flats of depth 2 mm at four speeds.

It can be seen that the main components of the impact force are in the region 100–1000 Hz. Below about 100 Hz the force spectrum decreases slightly with increasing

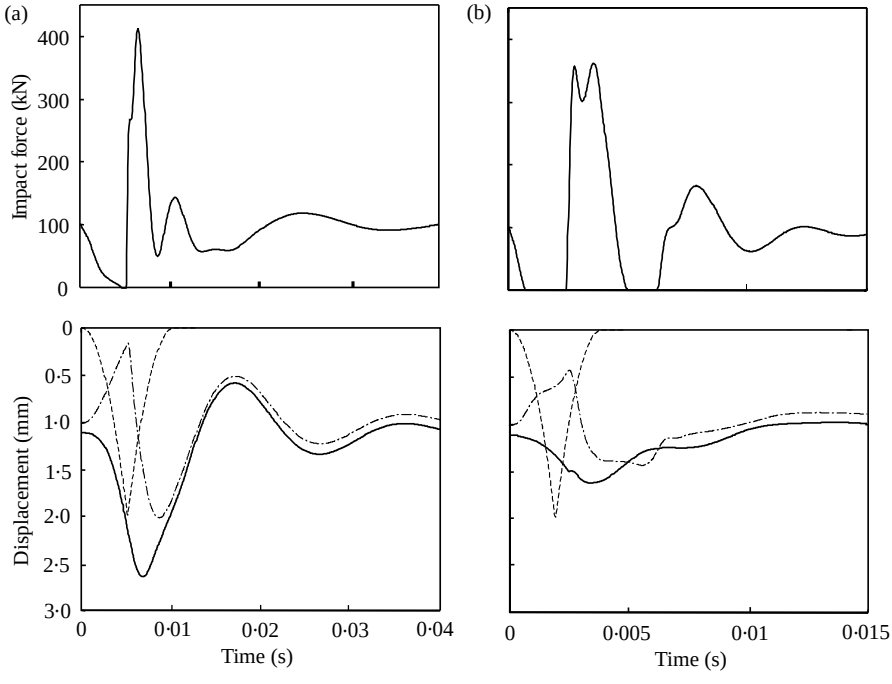

Figure 11. Wheel/rail interaction force and displacements of wheel and rail due to 2 mm newly formed wheel flat, key as for Figure 10.

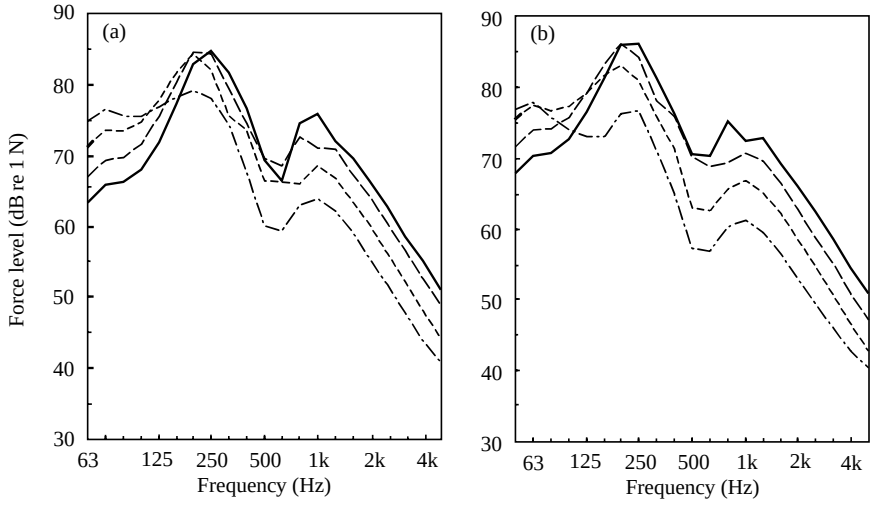

Figure 12. One-third octave spectra of the impact force caused by wheel flats at different train speeds. (a) Due to 2 mm newly formed flats. (b) Due to 2 mm rounded flats: ——, at 120 km/h; – – –, at 80 km/h, ·····, at 50 km/h, –·–·–, at 30 km/h.

speed. At high frequencies, the level increases considerably as the speed increases due to the shortening of the impact force pulse. This is more noticeable in the case of the rounded flat (Figure 12(b)).

These results illustrate that, in general, the impact force caused by wheel flats is related to both the shape of the flat and the train speed. The peak forces at different train speeds are

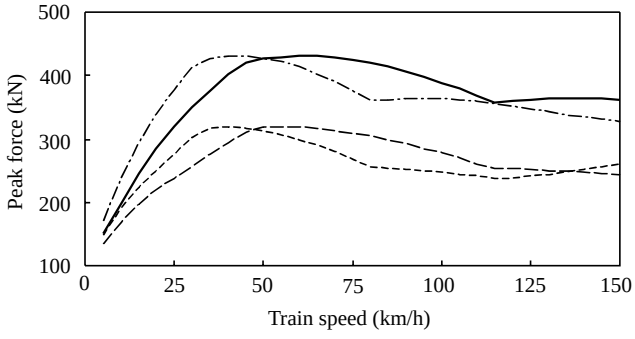

Figure 13. Peak impact force caused by different wheel flats: ——, due to 2 mm rounded flat; – – –, 1 mm rounded flat; – · – · –, 2 mm newly formed flat; ·····, 1 mm newly formed flat.

presented in Figure 13 for the wheel flats of different types and size. Two flat types are considered here, based on equation (4): a rounded one ($l = 121$ mm for $d = 2$ mm) and the newly formed one ($l = 86$ mm for $d = 2$ mm). Two flat depths are chosen for each type: $d = 1$ and 2 mm. At low speeds the peak forces increase with increasing speed and they are larger for the newly formed flats than for the rounded flats. For a given flat depth the peak forces are the same for both types of flat considered but these maxima are reached at higher speed for the rounded flats. This is a consequence of the fact that equation (4) is used in both cases. At higher speeds they decrease to slightly lower levels. At high speeds the peak forces are smaller for the newly formed flats than for the rounded flats. It can also be observed from Figure 13 that the deeper the wheel flats are, the larger are the impact forces. The shape of the curves here differs from that in Figure 9 due to the difference in the excitation function used.

5. A HYBRID METHOD FOR PREDICTING VIBRATION AND NOISE FROM WHEEL FLATS

5.1. BACKGROUND

The modelling so far has concentrated on the response of the wheel/rail system at the contact zone to the excitation from a wheel flat. The vibration so generated will be transmitted in the form of structural waves through the track which will radiate noise; it will also excite modes of vibration of the wheel which will radiate noise. Suitable models for the prediction of structural response and sound radiation of tracks and wheels are available within the TWINS model [6, 7] which is used for predicting rolling noise due to random roughness excitation. These models operate in the frequency domain and are normally used with a linear interaction model, so they cannot be used directly here.

One aspect required in order to predict the noise radiation due to wheel flat excitation, is that account should be taken of the modal behaviour of the wheel. It is known from studies of rolling noise that the wheel modes containing a significant radial component of motion at the contact zone dominate the noise radiation of the wheel/rail system in the frequency region above about 2 kHz [12]. The inclusion of all such modes in the time-domain model of wheel/rail interaction has not been considered in the present work, since there are many such modes and these have very light damping (loss factors around 10^{-4}). Consequently, they have a large time constant and numerical integration of the response becomes difficult.

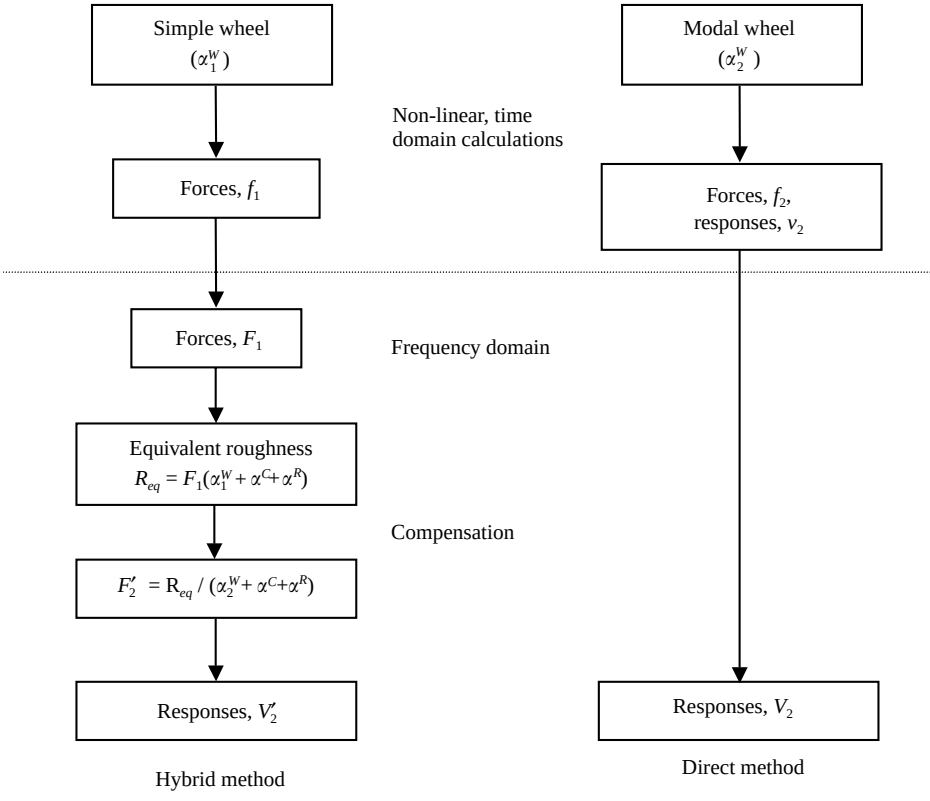

Figure 14. An overview of the hybrid method.

The proposed method of overcoming this difficulty is referred to here as a hybrid method and is summarized in Figure 14. The interaction force from a wheel flat is calculated first in the time domain by using the simple wheel model described above. Then, after conversion of this result to the frequency domain, this is applied as an excitation to a more complete model of the wheel and rail, as described in more detail in the following sections. However, as will be explained, it is essential in this hybrid approach that the force is first converted to an equivalent roughness.

5.2. CONTACT FORCE AND EQUIVALENT ROUGHNESS

It is known from rolling noise studies that the interaction force depends on the wheel and track dynamic properties as well as the roughness input. For a roughness excitation $R(\omega)$, at angular frequency ω, and considering only interaction in the vertical direction, the interaction force $F(\omega)$ is given by

$$F(\omega) = -\frac{R(\omega)}{\alpha^W(\omega) + \alpha^C(\omega) + \alpha^R(\omega)}, \tag{9}$$

where α^W, α^C and α^R are the receptances of the wheel, the contact spring and the rail respectively.

At a wheel resonance, the denominator is large due to a sharp peak in the wheel receptance. Consequently, the contact force has a sharp minimum at this frequency, and in

the wheel response this partially cancels the peak in the wheel receptance. Although the wheel response spectrum during rolling has peaks corresponding to each resonance of the wheel, their amplitude and bandwidth are consistent with a much higher level of damping than is present in the free wheel. This phenomenon is sometimes referred to as "rolling damping" [13].

For interaction in multiple degrees of freedom (d.o.f.), the situation is less straightforward, with the force component in the lateral direction cancelling that in the vertical direction rather a simple minimum occurring in the force amplitude at wheel resonances. Nevertheless, it remains true that, in the vicinity of wheel resonances, the force spectrum depends strongly on the wheel receptance. The use of a force spectrum calculated from a different wheel model would prevent this matching of the force spectrum with the wheel receptance and would produce wheel vibration estimates that are too high, since they effectively ignore the rolling damping.

It follows that the interaction force estimated when using a simple mass/spring model for the wheel, such as Figure 7, cannot be applied to a modal model of the wheel to calculate its response. Instead, it is possible to convert the interaction force back to an "equivalent roughness" spectrum—the roughness (relative displacement) input between the wheel and rail models that would produce the same force spectrum *if the contact spring were linear*. This is obtained by calculating the Fourier transform of the interaction force and using equation (9) in reverse to derive an equivalent roughness spectrum:

$$R_{eq}(\omega) = -F(\omega)(\alpha^{W}(\omega) + \alpha^{C}(\omega) + \alpha^{R}(\omega)). \tag{10}$$

The question that remains is whether the same equivalent roughness would be obtained if the high-frequency modal behaviour of the wheel were taken into account. In other words, are high-frequency oscillations in the contact force induced by wheel modes independent of the non-linear effects, which occur essentially at low frequencies? It will be demonstrated that this is the case in the following section by using an example.

5.3. SIMULATIONS USING A SIMPLIFIED MODAL WHEEL MODEL

A model is now considered for the wheel which contains a single lightly damped mode; this comprises three masses, two springs and two dampers, as shown in Figure 15. This system is referred to as a simplified modal wheel. Its receptance is shown as the solid line in Figure 8. Comparing this result with that from the full finite element wheel model, it can be seen that good agreement is found up to about 2 kHz, including the first main, lightly damped, resonance at high frequency (1688 Hz).

Two methods are now used to determine the response of this wheel to a wheel flat input and their results compared. The first is direct integration in the time domain by using the Runge–Kutta method, indicated by the right-hand side of Figure 14. The second is the proposed hybrid method, indicated by the left-hand side of Figure 14. In this, the wheel–rail contact force is calculated in the time domain using the mass–spring wheel model (Figure 7); this force is transformed into the frequency domain and then converted back to an equivalent roughness spectrum, R_{eq}, by using equation (10); this roughness is then applied in the frequency domain as the excitation of a wheel–rail system containing the modal wheel of Figure 15.

Figure 16 shows an example result for a 2 mm new flat, a wheel load of 50 kN and a train speed of 80 km/h. The graph shows the wheel velocity spectrum at the contact point. The result from the two methods (direct and hybrid) agree closely. Also shown is the result initially obtained for the mass/spring wheel model, showing the extent of the correction

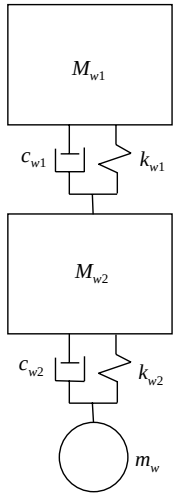

Figure 15. Simplified modal wheel model. $M_{w1} = 400$ kg, $M_{w2} = 200$ kg, $m_w = 3$ kg, $k_{w1} = 15$ GN/m, $k_{w2} = 5{\cdot}92$ GN/m, and respective damper rates $c_{w1} = 0{\cdot}245$ kN s/m and $c_{w2} = 54{\cdot}4$ kN s/m.

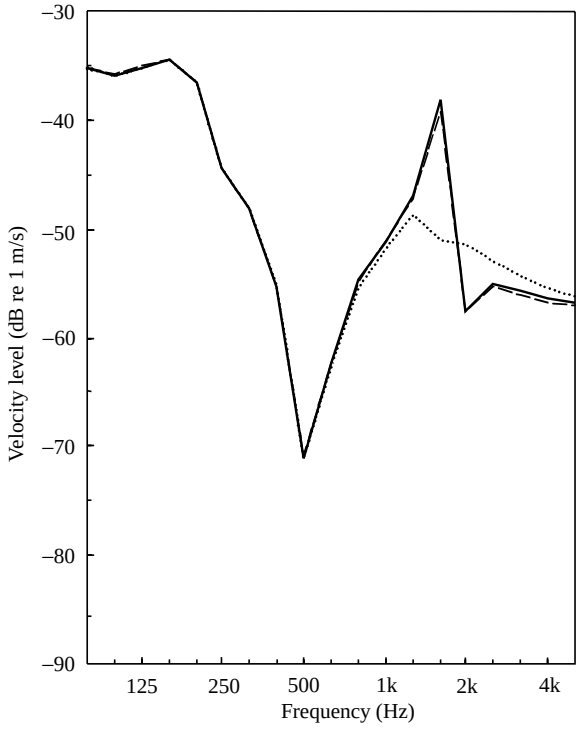

Figure 16. Wheel velocity spectrum at the contact point for a 2 mm new flat, a wheel load of 50 kN and a train speed of 80 km/h for the simplified modal wheel: ——, from the direct method; – – –, from the hybrid method; ·····, for the mass/spring wheel before correction is applied.

applied by the hybrid method. This correction is small below 1 kHz, but up to 12 dB in the band containing the resonance.

These calculations have been repeated for loads of 25, 50 and 100 kN, for speeds of 40, 80 and 160 km/h and for new wheel flats of 1 and 2 mm depth. The differences found are shown

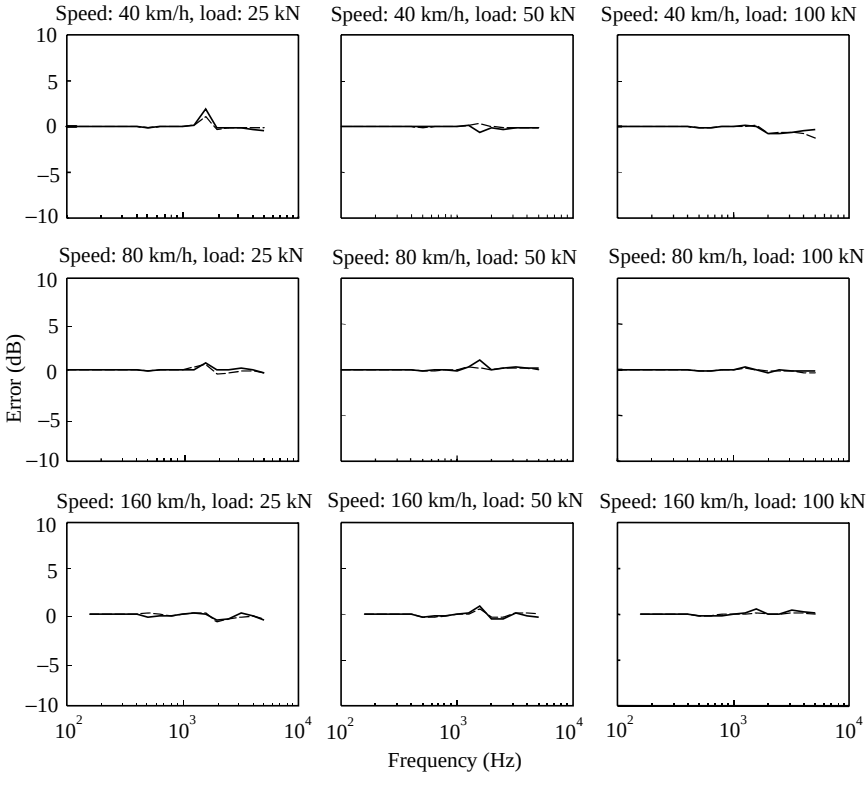

Figure 17. Difference between the wheel velocity of the simplified modal wheel obtained by the direct and hybrid methods: ——, 2 mm new flat; – – –, 1 mm new flat.

in Figure 17. These differences represent the error introduced by using the hybrid method. This error is very small for frequencies less than 1600 Hz. The band containing the lightly damped resonance is the only band containing significant error—the error in this band is found to be less than 2 dB in every case. For a full wheel model containing many modes, it can be expected that a similar level of agreement will be found in the whole of the modal region, i.e., above 1·6 kHz.

6. APPLICATION TO NOISE FROM WHEEL FLATS

6.1. IMPACT FORCE IN THE FREQUENCY DOMAIN AND EQUIVALENT ROUGHNESS INPUT

In this section the hybrid method introduced above will be used to calculate the noise radiated by a wheel and the track due to excitation by a wheel flat. The impact force is calculated in the time domain as in section 4.3. Figure 12 shows the force spectra produced from new and rounded flats of depth 2 mm at four speeds.

By using equation (10) these force spectra can be converted to an equivalent roughness. This is performed at the discrete frequencies of the periodic force spectrum and the resulting equivalent roughness spectrum is then converted to one-third octave form. The equivalent roughness spectra corresponding to the force spectra of Figure 12(a) are shown in Figure 18. Similar trends can be seen, since the same conversion is applied in each case.

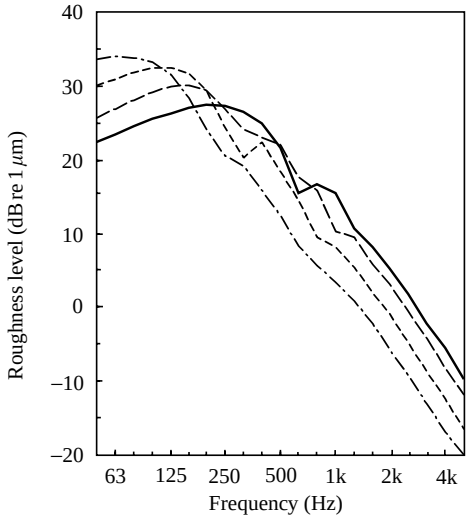

Figure 18. One-third octave spectra of the equivalent roughness due to 2 mm newly formed wheel flats at different train speeds: ——, at 120 km/h; – – –, at 80 km/h; ·····, at 50 km/h; – · – ·, at 30 km/h.

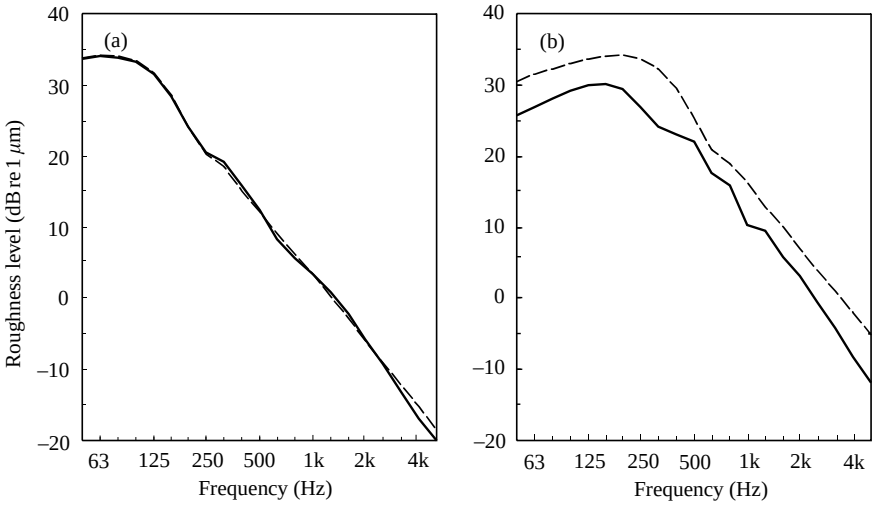

Figure 19. Comparison of one-third octave spectra of the equivalent roughness due to 2 mm newly formed flats with the original displacement input. (a) At 30 km/h. (b) At 80 km/h. ——, equivalent roughness excitation; – – –, original displacement input.

In Figure 19 two of these curves are compared with the spectrum of the original relative displacement input used in each case, i.e., based on equation (4). At a speed of 30 km/h, the equivalent roughness spectrum is very similar to the spectrum of the original input, even though from Figure 11(a) it can be seen that loss of contact occurs momentarily and the maximum contact force is more than four times the nominal load of 100 kN. From this it is clear that, provided loss of contact does not occur, (1) the equivalent roughness can be taken directly from the wheel flat geometry, modified to allow for the curvature of the wheel, and (2) the non-linear contact stiffness can be replaced by an equivalent linear spring. The latter conclusion has already been drawn in relation to random roughness inputs [11].

At 80 km/h, however, the equivalent roughness spectrum is about 3–5 dB lower than the spectrum of the original input. Figure 11(b) shows that contact is lost twice during the wheel flat event for a period of between 1 and 2 ms. The first loss of contact occurs during the maximum part of the input irregularity. This means that this part of the irregularity does not excite the wheel/rail system; the shape of the irregularity during loss of contact is actually arbitrary and therefore does not contribute to the excitation. It is therefore not possible to find the equivalent roughness without performing the non-linear dynamic wheel/rail interaction calculations for this case.

6.2. IMPACT NOISE DUE TO WHEEL FLATS

The equivalent roughness spectra derived in the previous section are now used as inputs to a frequency-domain calculation of wheel/rail noise. For this, the TWINS model [6, 7] is used. The wheel is represented by its full modal basis in the frequency range up to 6 kHz, determined from a finite element model. The track is modelled by a Timoshenko beam continuously supported on layers of damped springs and mass (see Figure 6). Track parameters are as listed in Table 1. Wheel/rail interaction is included in both vertical and lateral directions, the excitation being due to the equivalent roughness acting in the vertical direction.

Figure 20(a) shows the predicted overall sound power radiated by one wheel and the associated track vibration for new flats of 2 mm depth at various speeds. As the speed increases, the noise increases at frequencies above about 200–400 Hz.

These results may be compared with Figure 20(b) which shows the sound power predicted for the same wheel/track combination from typical roughness spectra. This roughness represents cast-iron tread-braked vehicles on good-quality track. For the wheel flat that has been considered, the noise generated exceeds that due to the tread-braked wheel roughness at all speeds and in all frequency bands, although the noise due to roughness increases more rapidly with speed so that at sufficiently higher speeds it can be

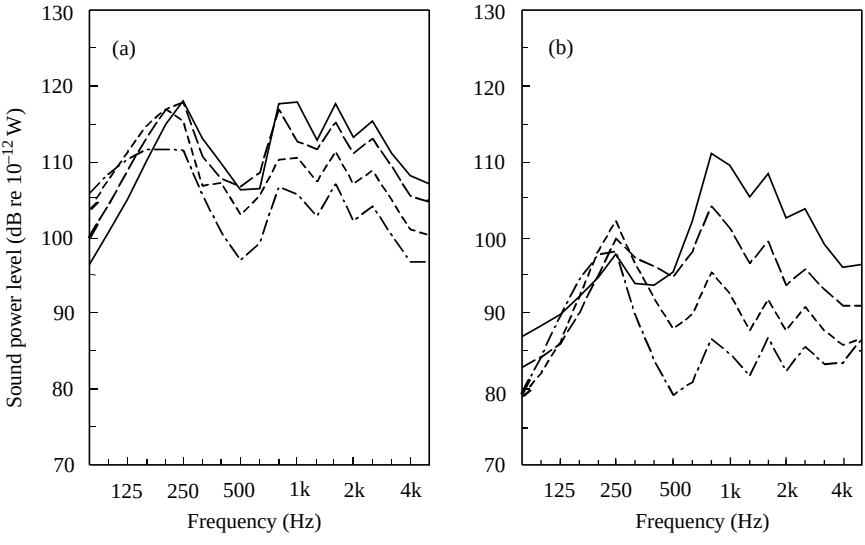

Figure 20. Sound power level due to wheel and track. (a) From a 2 mm new wheel flat. (b) From the roughness on a typical tread-braked wheel: –·–·–, 30 km/h; ·····, 50 km/h; – – –, 80 km/h, ——, 120 km/h.

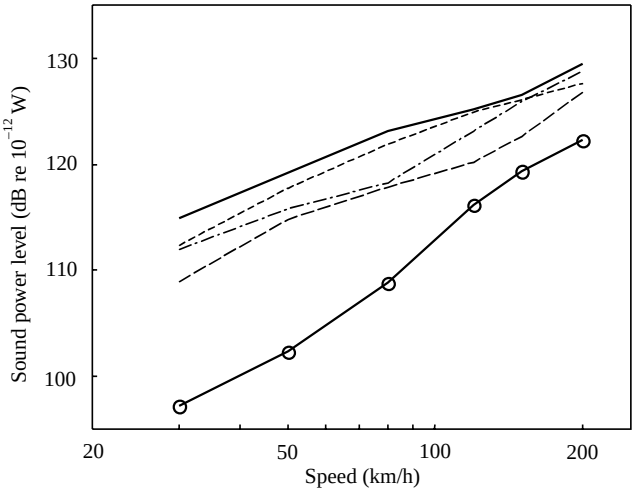

Figure 21. *A*-weighted sound power radiated by one wheel and the associated track vibration: – – –, 1 mm rounded flat; ·····, 2 mm rounded flat; – · – · –, 1 mm new flat; ——, 2 mm new flat, ○---○, rolling noise due to roughness (tread-braked wheel).

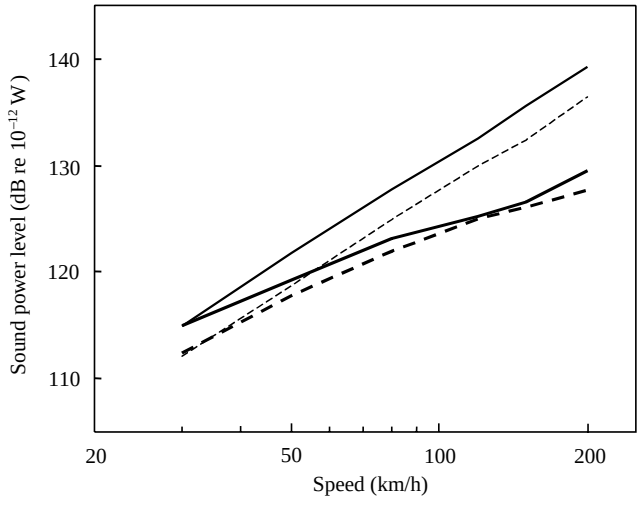

Figure 22. A-weighted sound power radiated by one wheel and the associated track vibration due to flats: ·····, 2 mm rounded flat; ——, 2 mm new flat. Thick lines: from equivalent roughness, thin lines from original relative displacement input.

expected to dominate. For a high rail roughness, as found on a corrugated track, the noise due to roughness has been found to exceed that due to these wheel flats at 120 km/h.

Figure 21 shows a summary of the variation of the overall *A*-weighted sound power level with train speed for various wheel flats. The predicted noise level due to roughness excitation increases at a rate of approximately $30 \log_{10} V$, where V is the train speed, whereas the noise due to flats is higher but increases at an average of only around $20 \log_{10} V$. This variation with speed indicates that the radiated sound due to wheel flats continues to increase with increasing speed, even though loss of contact is occurring. For example, loss of contact is found to occur for the newly formed 2 mm flat at speeds above 30 km/h and for the rounded 2 mm flat above 50 km/h.

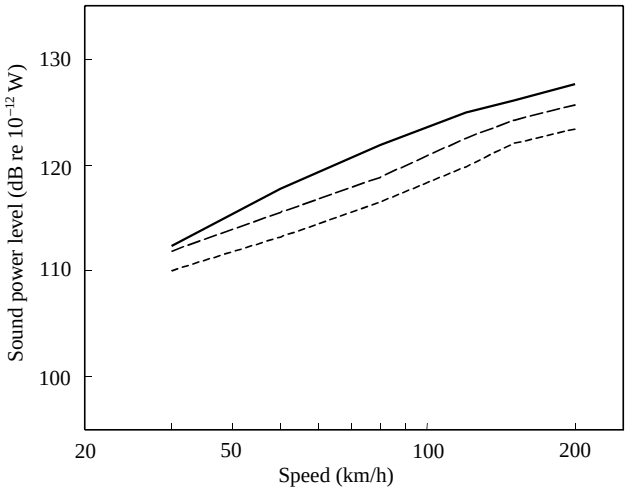

Figure 23. A-weighted sound power radiated by one wheel and the associated track vibration for a 2 mm rounded flat: ——, for 100 kN wheel load; – – –, for 50 kN wheel load; ·····, for 25 kN wheel load.

Below these speeds, as shown in Figure 19, the equivalent roughness closely follows the original relative displacement input. Figure 22 shows the impact noise predicted from the original relative displacement input for a range of speeds. Compared to the equivalent roughness, this gives a higher noise level once loss of contact occurs and its slope is close to $30 \log_{10} V$. For lower speeds, although not predicted, the $30 \log_{10} V$ curves can be expected to apply. According to Vér *et al.* [4] the noise was expected to reach a constant level when loss of contact occurs. The results here, however, which are based on a more comprehensive model, do not support this. Above the critical speed of Vér *et al.*, a change occurs in the slope of noise level with speed, but a constant level is not reached.

All the results presented so far in this section have been for a wheel load of 100 kN. For lower wheel loads, the likelihood of loss of contact is increased [11]. At low speeds, where contact is not lost, the equivalent roughness will closely follow the spectrum of the displacement input (Figure 19) and so the results for different wheel loads will be similar. At higher speeds, greater loss of contact will occur for lower wheel loads and therefore the noise level will be lower.

Figure 23 shows the overall *A*-weighted sound power level plotted against train speed for a 2 mm rounded flat at three values of wheel load. The corresponding TWINS calculations include the effect of the change in the contact stiffness. For 25 and 50 kN loads, loss of contact occurs for all speeds considered, whereas for 100 kN it only occurs at 50 km/h and above. For most of the results shown here, therefore, the noise level reduces as the wheel load is reduced. For a halving of the wheel load, the noise level due to the flat is reduced by about 3 dB. This corresponds to the difference between typical passenger vehicles (50 kN) and loaded freight vehicles (100 kN). In contrast, rolling noise due to roughness is relatively insensitive to variations in the wheel load, changing by only 0·7 dB between 50 and 100 kN due to a change in contact stiffness.

7. CONCLUSIONS

A numerical model has been developed to predict the wheel/rail dynamic interaction due to wheel-flat excitation. The form of the relative displacement excitation between the wheel

and rail differs from the profile of the wheel flat due to the finite curvature of the wheel. To allow for the non-linear contact spring, and the possibility of loss of contact between the wheel and the rail, a time-domain model is required. For this, simplified dynamic models of the wheel and the track are used with a non-linear model of the contact spring between them. Results have been compared with published measurement data and shown to be in good agreement. For a newly formed wheel flat, of depth 2 mm and length 86 mm, loss of contact is found to occur for speeds above 30 km/h. For a rounded flat of the same depth but overall length 121 mm the speed at which loss of contact first occurs increases to about 50 km/h. At higher speeds a second loss of contact occurs after the initial impact.

In order to predict the consequent noise radiation, the wheel/rail interaction force is transformed into the frequency domain, and then converted back to an equivalent roughness spectrum. This spectrum is used as the excitation to a linear, frequency-domain model of wheel/rail interaction to predict the noise. This hybrid approach has been shown to be adequate by comparing direct and hybrid calculations for a wheel with a single, lightly damped resonance.

As the train speed increases, the force spectrum and consequently the noise radiation, contains greater amplitudes at high frequencies and the overall noise level due to wheel flat excitation increases with the train speed V at a rate of roughly $20 \log_{10} V$ once loss of contact occurs. This differs from rolling noise due to roughness excitation which generally increases at $30 \log_{10} V$. The noise from flats of depth 1 and 2 mm exceeds that due to typical roughness on tread-braked wheels and good-quality track for all speeds up to at least 200 km/h. The results do not show a critical speed above which the level remains constant, as suggested by Vér *et al.* [4].

As the wheel load increases, the noise from wheel flats increases. The difference between a load of 50 kN, typical of passenger stock, and 100 kN, typical of loaded freight vehicles, is about 3 dB. In contrast, the rolling noise due to roughness is relatively insensitive to wheel load.

ACKNOWLEDGMENTS

The work described has been performed within the project "Non-linear Effects at the Wheel/rail Interface and their Influence on Noise Generation" funded by EPSRC (Engineering and Physical Sciences Research Council of the United Kingdom), grant GR/M82455.

REFERENCES

1. J. JERGÉUS 1998 *Ph.D. Thesis, Chalmers University of Technology, Gothenburg, Sweden.* Railway wheel flats—martensite formation, residual stresses and crack propagation.
2. S. G. NEWTON and R. A. CLARK 1979 *Journal of Mechanical Engineering Science* **21**, 287–297. An investigation into the dynamic effects on the track of wheelflats on railway vehicles.
3. Joint Committee on Relation between Track and Equipment of the Mechanical and Engineering Divisions, AAR 1952 *American Railway Engineering Association* **53**, 423–448. Effect of flat wheels on track and equipment (abstract of report)
4. I. L. VÉR, C. S. VENTRES and M. M. MYLES 1976 *Journal of Sound and Vibration* **46**, 395–417. Wheel/rail noise. Part III: impact noise generation by wheel and rail discontinuities.
5. P. J. REMINGTON 1987 *Journal of Sound and Vibration* **116**, 339–353. Wheel/rail squeal and impact noise: what do we know? What don't we know? Where do we go from here?
6. D. J. THOMPSON and M. H. A. JANSSENS 1997 *TNO Institute of Applied Physics Report TPD-HAG-RPT-93-0214, Delft.* TWINS: track-wheel interaction noise software. Theoretical manual (version 2.4).

7. D. J. THOMPSON, B. HEMSWORTH and N. VINCENT 1996 *Journal of Sound and Vibration* **193**, 123–135. Experimental validation of the TWINS prediction program for rolling noise. Part 1: description of the model and method.
8. D. J. THOMPSON 1996 *Journal of Sound and Vibration* **193**, 149–160. On the relationship between wheel and rail surface roughness and rolling noise.
9. P. J. REMINGTON and J. WEBB 1996 *Journal of Sound and Vibration* **193**, 83–102. Estimation of wheel/rail interaction forces in the contact area due to roughness.
10. S. L. GRASSIE, R. W. GREGORY, D. HARRISON and K. L. JOHNSON 1982 *Journal of Mechanical Engineering Science* **24**, 77–90. The dynamic response of railway track to high frequency vertical excitation.
11 T. X. WU and D. J. THOMPSON 2001 *Vehicle System Dynamics* **34**, 261–282. Theoretical investigation of wheel/rail non-linear interaction due to roughness excitation.
12. D. J. THOMPSON and C. J. C. JONES 2000 *Journal of Sound and Vibration* **231**, 519–536. A review of the modelling of wheel/rail noise generation.
13. D. J. THOMPSON 1993 *Journal of Sound and Vibration* **161**, 467–482. Wheel–rail noise generation. Part V: inclusion of wheel rotation.

APPENDIX A. WHEEL CENTRE TRAJECTORY FOR AN IDEALIZED ROUNDED FLAT

For a region of the wheel surface that is small compared with the wheel radius, a round wheel can be represented approximately by a quadratic function. A flat portion of the wheel surface therefore has a profile height, that is the difference between the actual profile and the perfectly round wheel, which is quadratic with the same curvature as the wheel but in the opposite direction, see equation (3).

Consider a rounded wheel flat of depth d, and overall length l. The corresponding profile height is shown schematically in Figure A1, with an indentation shown as positive and downwards. In the region between z_1 and z_3 the wheel surface is flat, so that the profile height has the same curvature as the wheel. Between $z = 0$ and z_1 and between z_3 and l a transition is defined by a quadratic function such that the gradient is continuous.

From these assumptions, the wheel profile depth can be written as

$$x_p(z) = \begin{cases} az^2, & 0 \leqslant z \leqslant z_1 \\ d - \dfrac{1}{2r}(z - z_2)^2, & z_1 \leqslant z \leqslant z_2 \end{cases}, \tag{A1}$$

where $z = z_2 = l/2$ is the point at the centre of the flat, $z = z_1$ is the point at which the two curves meet, and a is a constant determining the extent of the transition. For $z < 0$, $x_p = 0$, while for $z > z_2$, $x_p(z) = x_p(2z_2 - z)$. At $z = z_1$ it is required that x_p and its first derivative are continuous. This gives two equations relating a, z_1 and z_2:

$$2az_1 = \frac{(z_2 - z_1)}{r}, \qquad az_1^2 = d - \frac{(z_2 - z_1)^2}{2r}. \tag{A2, A3}$$

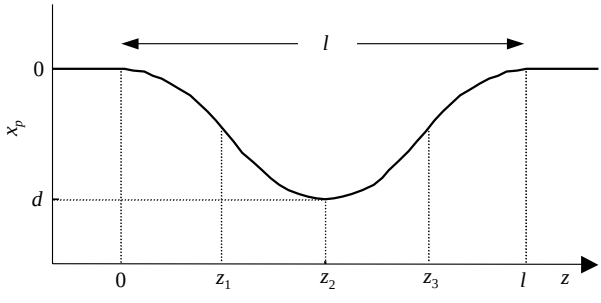

Figure A1. Idealized "rounded flat" profile.

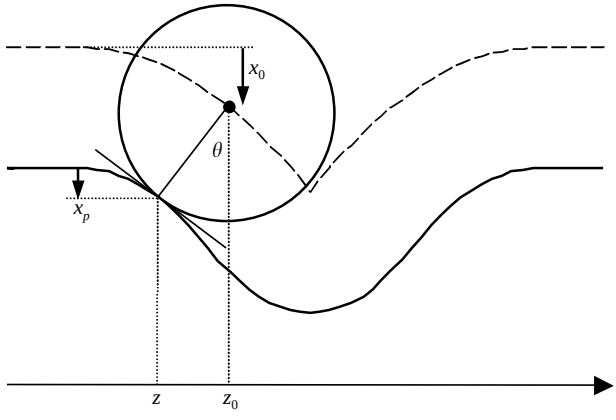

Figure A2. Rolling of a wheel on an idealized "rounded flat" profile.

These can be rearranged to give

$$z_1 = \frac{z_2}{2ar + 1}, \tag{A4}$$

$$d = az_1^2(2ar + 1) = \frac{az_2^2}{2ar + 1}. \tag{A5}$$

Provided that the flat is short compared to the wheel radius, the same excitation of the wheel/rail system occurs whether the profile x_p is applied as an indentation on the rail surface or on the wheel. By considering it to be on the rail, this allows the wheel centre trajectory to be determined more readily, as follows.

As a round wheel rolls over a rail with the profile x_p, the wheel surface and the rail profile share a common tangent, see Figure A2. When the contact is at a distance z along the rail, the gradient of this tangent is

$$\theta \approx \tan\theta = x_p'(z) = 2az \tag{A6}$$

and the wheel centre is located at

$$z_0 = z + r\sin\theta \approx z(1 + 2ar). \tag{A7}$$

From equations (A4) and (A7), when the contact point is at $z = z_1$, the wheel centre is at $z_0 = z_2$, at which point the contact jumps to z_3. The height of the wheel centre is thus given by

$$x_0(z_0) = x_p(z) + r(1 - \cos\theta) \approx az^2 + r\,\theta^2/2,$$

$$x_0(z_0) \approx az^2(1 + 2ar). \tag{A8}$$

Upon rewriting this in terms of z_0 (from equation (A7)),

$$x_0(z_0) \approx az_0^2/(1 + 2ar) \tag{A9}$$

and, from equation (A5), the wheel centre trajectory can be written as

$$x_0(z_0) = d\frac{z_0^2}{z_2^2} = 4d\frac{z_0^2}{l^2}, \qquad 0 \leqslant z_0 \leqslant l/2. \tag{A10}$$

By symmetry, $x_0(z_0) = x_0(l–z_0)$ for $l/2 \leqslant z_0 \leqslant l$.